# Residual-based a posteriori error analysis of a Taylor–Hood discretization of the Reissner–Mindlin plate

D. Gallistl* M. Schedensack†

17th March 2025

**Abstract**

For a discretization of the Reissner–Mindlin plate model proposed by the authors in [SIAM J. Numer. Anal. 59(3), 2021], a residual-based a-posteriori error estimator is proven to be reliable and efficient. The estimates are robust in the plate thickness parameter. Numerical experiments assess the behaviour of the individual error estimator components and the application to adaptive mesh refinement.

**Keywords.** a posteriori, Reissner–Mindlin, adaptivity, Taylor–Hood
**AMS subject classification.** 65N12, 65N15, 65N30, 74K20

## 1 Introduction

The use of the Helmholtz decomposition of the shear force in the Reissner–Mindlin plate model [BF86] revealed a structure that established a guideline for shear-locking free discretizations. This structure is preserved in the low-order nonconforming method of [AF89a] in a pointwise sense thanks to a discrete Helmholtz decomposition established by those authors. For that method, [Car02] proved residual-based a posteriori error estimates. A higher-order generalization of the method [AF89a] was proposed in [GS20, GS21] based on a generalization [Sch17] of the Crouzeix–Raviart method. What makes the method from [GS21] attractive is that it is based on the generalized Taylor–Hood pair [BBF13] and therefore on standard trial spaces. Moreover, the rotation employs the full approximation properties of the Taylor–Hood space. The interplay of local forces, corner singularities, and boundary layers of different strengths depending on the boundary conditions makes a priori mesh grading very challenging, in particular for high-order methods. In order to explore the possibility of adaptive mesh refinement, in this work we prove the reliability and efficiency of

*Institut für Mathematik, Universität Jena, 07743 Jena, Germany; E-mail: dietmar.gallistl (at) uni-jena.de; Supported by the European Research Council (ERC Starting Grant *DAFNE*, ID 891734).

†Mathematisches Institut, Universität Leipzig, PF 10 09 20, 04009 Leipzig, Germany; E-mail: mira.schedensack (at) math.uni-leipzig.de; Supported by the DFG Priority Program 1748 under the project "Robust and Efficient Finite Element Discretizations for Higher-Order Gradient Formulations" (SCHE1885/1-1).

a residual-based a posteriori error estimator for the methods of [GS20, GS21]. The methods are based on an alternative formulation related to the Schur complement of some mixed system. Given an open, bounded, simply connected polygonal domain $\Omega \subseteq \mathbb{R}^2$, and the load function $\ell \in L^2(\Omega)$, the classical Reissner–Mindlin model [BBF13, Bra07] seeks the displacement $w \in H^1_0(\Omega)$ and the rotation $\phi \in [H^1_0(\Omega)]^2$ such that

$$a(\phi, \psi) + \lambda t^{-2}(\nabla w - \phi, \nabla v - \psi)_{L^2(\Omega)} = (\ell, v)_{L^2(\Omega)} \tag{1}$$

for all $(v, \psi) \in H^1_0(\Omega) \times [H^1_0(\Omega)]^2$. Here, $t > 0$ is the plate thickness and the bilinear form $a(\cdot, \cdot)$ is defined by $a(\phi, \psi) := (\varepsilon(\phi), \mathbb{C}\varepsilon(\psi))_{L^2(\Omega)}$ for the linear Green strain $\varepsilon(\cdot) = \operatorname{sym} D(\cdot)$ and the linear elasticity tensor $\mathbb{C}$ that acts on any symmetric matrix $A \in \mathbb{R}^{2\times 2}$ as follows

$$\mathbb{C}A = \frac{E}{12(1-\nu^2)}((1-\nu)A + \nu \operatorname{tr}(A) I_{2\times 2})$$

with Young's modulus $E > 0$ and the Poisson ratio $0 < \nu < 1/2$. The constant $\lambda$ in (1) reads $\lambda = (1+\nu)^{-1} E\kappa/2$ with a shear correction factor $\kappa$ usually chosen as $5/6$. The method of [GS21] considered here and described in Section 2 below involves $\phi$ and a scalar-valued variable $\alpha$ with boundary values complementary to those of $w$, and a vector field $\eta$ with the property $-\operatorname{div} \eta = \ell$. They are directly related to the shear force by $\zeta = \eta - \operatorname{Curl} \alpha$, with analogous discrete relations, and therefore these nonstandard variables directly enter the error estimator based on residuals of the stress (and thus $\phi$) and the shear force $\zeta$. Although the displacement $w$ can be recovered from the system, it is not further relevant for a posteriori error estimation. The results generalize the low-order case considered in [Car02]. In particular, the efficiency proof presented here differs from [Car02], is based on locally adapted bubble functions following [Ver98, Ver13] (also employed in [CS06, HH10]), and applies to more general boundary conditions as discussed in Section 2.4. For a posteriori error estimates and adaptive computations with alternative methods we refer to [CW03, CW01, CH08].

The remaining parts of this article are organized as follows. Section 2 revisits the alternative formulation and discretization of [GS21], states the main result, namely the residual-based a posteriori error estimate, and comments on the application to more general boundary conditions. The proof of the main result is given in Section 3, where the system is considered in a non-dimensional form in order to focus on robustness with respect to the critical parameters in the system. The numerical experiments of Section 4 conclude the paper. Appendix A collects certain longer formulas.

Standard notation on Lebesgue and Sobolev spaces applies throughout this paper. The $L^2$ inner product is denoted by $(v, w)_{L^2(\omega)}$ for a domain $\omega \subseteq \Omega$ and $\|\bullet\|_\omega := \|\bullet\|_{L^2(\omega)}$ and $\|\bullet\| := \|\bullet\|_\Omega$ denote the $L^2$ norm. The $H^k$ seminorm over $\omega \subseteq \Omega$ is denoted by $|\bullet|_{k,\omega}$ and $|\bullet|_k := |\bullet|_{k,\Omega}$. The space of $H^1(\Omega)$ functions with vanishing global average is denoted by $H^1(\Omega)/\mathbb{R}$. For a function $v$ and a vector field $\psi$, the following differential operators are defined

$$\operatorname{div} \psi = \partial_1 \psi_1 + \partial_2 \psi_2, \quad \operatorname{rot} \psi = \partial_1 \psi_2 - \partial_2 \psi_1, \quad \operatorname{Curl} v = \begin{pmatrix} -\partial_2 v \\ \partial_1 v \end{pmatrix}.$$

The notation $A \lesssim B$ abbreviates $A \leq CB$ for some constant $C$ that is independent of the mesh size, the plate's thickness $t$, and Young's modulus $E$ (but it may depend on the fixed constant $\kappa$ and on the bounds 0 and 1/2 of $\nu$). The notation $A \approx B$ abbreviates $A \lesssim B \lesssim A$.

# 2 Discretization and a posteriori error estimate

## 2.1 Equivalent formulation

The a posteriori error analysis below will rely on a reformulation of the Reissner–Mindlin equation (1) that is based on $\eta \in H(\mathrm{div}, \Omega)$ satisfying $-\operatorname{div} \eta = \ell$, which can be computed based on $\ell$. Define the bilinear forms $b : L^2(\Omega; \mathbb{R}^2) \times H^1(\Omega) \to \mathbb{R}$ and $c : H^1(\Omega) \times H^1(\Omega) \to \mathbb{R}$ by

$$\begin{aligned} b(\psi, \beta) &= (\psi, \operatorname{Curl} \beta)_{L^2(\Omega)}\,, \\ c(\alpha, \beta) &= (\operatorname{Curl} \alpha, \operatorname{Curl} \beta)_{L^2(\Omega)}\,. \end{aligned}$$

The introduction of a Lagrange multiplier $\alpha \in H^1(\Omega)/\mathbb{R}$ in the Schur complement of [GS21] yields the problem: Find $(\phi, \alpha) \in [H^1_0(\Omega)]^2 \times H^1(\Omega)/\mathbb{R}$ with

$$\begin{aligned} a(\phi, \psi) + b(\psi, \alpha) &= (\eta, \psi)_{L^2(\Omega)} \\ b(\phi, \beta) - \lambda^{-1} t^2 c(\alpha, \beta)_{L^2(\Omega)} &= -\lambda^{-1} t^2 b(\eta, \beta) \end{aligned} \tag{2}$$

for all $(\psi, \beta) \in [H^1_0(\Omega)]^2 \times H^1(\Omega)/\mathbb{R}$. Note that this is a standard saddle point problem with penalty term [Bra07]. The following result from [GS21] proves the equivalence with (1) and provides the formula for the shear force.

**Theorem 1** ([GS21, Prop. 4.2])**.** *The problems* (1) *and* (2) *are equivalent in the following sense: If* $(\phi, w) \in [H^1_0(\Omega)]^2 \times H^1_0(\Omega)$ *is a solution of* (1)*, then there exists* $\alpha \in H^1(\Omega)/\mathbb{R}$ *such that* $(\phi, \alpha)$ *solves* (2)*. On the other hand, if* $(\phi, \alpha) \in [H^1_0(\Omega)]^2 \times H^1(\Omega)/\mathbb{R}$ *solves* (2)*, then there exists* $w \in H^1_0(\Omega)$*, such that* $(\phi, w)$ *solves* (1)*. Furthermore,* $w$ *and* $\alpha$ *satisfy*

$$\nabla w + \lambda^{-1} t^2 \operatorname{Curl} \alpha = \phi + \lambda^{-1} t^2 \eta$$

*and, therefore, the shear force is given by*

$$\zeta = \lambda t^{-2} (\nabla w - \phi) = \eta - \operatorname{Curl} \alpha. \tag{3}$$

## 2.2 Discretization

Let $\mathcal{T}$ be a regular triangulation of $\Omega$ from a shape-regular family, consisting of at least three triangles. Let $P_k(\mathcal{T})$ denote the space of piecewise polynomials of degree not larger than $k$ and let $\Pi_k$ denote the $L^2$ projection to $P_k(\mathcal{T})$. Further define

$$S^k(\mathcal{T}) := P_k(\mathcal{T}) \cap H^1(\Omega) \qquad \text{and} \qquad S^k_0(\mathcal{T}) := P_k(\mathcal{T}) \cap H^1_0(\Omega).$$

The discretization of (2) employs the following discrete spaces for $k \geq 0$

$$\begin{aligned} \Phi_h &:= S^{k+2}_0(\mathcal{T}; \mathbb{R}^2) \\ Q_h &:= S^{k+1}(\mathcal{T}) \cap H^1(\Omega)/\mathbb{R} \end{aligned}$$

and seeks $(\phi_h, \alpha_h) \in \Phi_h \times Q_h$ with

$$\begin{aligned} a(\phi_h, \psi_h) + b(\psi_h, \alpha_h) &= (\Pi_k \eta, \psi_h)_{L^2(\Omega)} \\ b(\phi_h, \beta_h) - \lambda^{-1} t^2 c(\alpha_h, \beta_h)_{L^2(\Omega)} &= -\lambda^{-1} t^2 b(\eta, \beta_h) \end{aligned} \tag{4}$$

for all $(\psi_h, \beta_h) \in \Phi_h \times Q_h$. Note that $\Phi_h$ and $Q_h$ are the stable (generalized) Taylor–Hood pair [BBF13] for the Stokes system.

The approximation $\zeta_h$ of the shear variable $\zeta$ is defined according to (3), namely

$$\zeta_h = \Pi_k \eta - \operatorname{Curl} \alpha_h \in P_k(\mathcal{T}; \mathbb{R}^2). \tag{5}$$

*Remark* 1. Similar to the continuous case, the discretization (4) is equivalent to a problem of the form: Find $(\sigma_h, \phi_h) \in Z_h \times \Phi_h$ such that for all $(\tau_h, \psi_h) \in Z_h \times \Phi_h$ there holds

$$a(\phi_h, \psi_h) + \lambda t^{-2} (\Pi_k \phi_h - \sigma_h, \Pi_k \psi_h - \tau_h)_{L^2(\Omega)} = (\eta, \tau_h)_{L^2(\Omega)}, \tag{6}$$

where

$$Z_h := \{\sigma_h \in P_k(\mathcal{T}; \mathbb{R}^2) \mid (\sigma_h, \operatorname{Curl} q_h)_{L^2(\Omega)} = 0 \text{ for all } q_h \in Q_h\}$$

denotes a space of discrete (nonconforming) gradients. Here, the $L^2$ projection $\Pi_k$ plays the role of a reduction or reduced integration operator. Such operators are commonly met in the discretization of Reissner–Mindlin plates [Bra07]. In the lowest-order case, $k = 0$, the discrete Helmholtz decomposition of [AF89a] shows that $Z_h$ equals the space of piecewise gradients of the nonconforming $P_1$ finite element functions [CR73]. According to (3), the approximation $\sigma_h$ of $\nabla w$ can be directly reconstructed by

$$\sigma_h = \Pi_k(\phi_h + \lambda^{-1} t^2 \eta) - \lambda^{-1} t^2 \operatorname{Curl} \alpha_h \in Z_h. \tag{7}$$

The equivalence is shown in [GS21, Prop. 4.3], compare also [GS20, Section 2.2.2] for a version formulated with matrices.

## 2.3 Main result

We are now in the position to define the error estimator for the discretization of (1). Let $\mathcal{E}$ denote the set of edges of $\mathcal{T}$ and $\mathcal{E}(\Omega)$ the set of interior edges. For any interior edge $F \in \mathcal{E}(\Omega)$ we fix the two triangles $T_+, T_- \in \mathcal{T}$ with $F = T_+ \cap T_-$, while for a boundary edge, let $T_+ \in \mathcal{T}$ be the unique triangle with $F \subseteq T_+$. Then, let $\nu_F = \nu_{T_+}|_F$ be the unit normal on $F$ and $\tau_F = (0, -1; 1, 0)\nu_F$ denotes the unit tangent on $F$. Furthermore, for an interior edge $F \in \mathcal{E}(\Omega)$, let $[v]_F := v|_{T_+} - v|_{T_-}$ denote the jump across $F$ and for a boundary edge $F \in \mathcal{E} \setminus \mathcal{E}(\Omega)$, let $[v]_F := v|_{T_+}$. The diameter of $T$ and $F$ is denoted by $h_T$ and $h_F$, respectively. Recall that $\zeta_h := \Pi_k \eta - \operatorname{Curl} \alpha_h$ denotes the discrete shear

force, see (5). For every $T \in \mathcal{T}$, we define the local error estimator contributions

$$\mu_1^2(T) := \frac{h_T^2}{E^2} \| - \operatorname{div} \mathbb{C}\varepsilon(\phi_h) - \zeta_h\|_T^2,$$

$$\mu_2^2(T) := \sum_{\substack{F \in \mathcal{E}(\Omega) \\ F \subseteq T}} \frac{h_F}{E^2} \|[\mathbb{C}\varepsilon(\phi_h)]_F \nu_F\|_F^2,$$

$$\mu_3^2(T) := \min\left\{1, \frac{h_T\sqrt{\lambda}}{t\sqrt{E}}\right\}^2 \left\|\operatorname{rot}\left(\phi_h + \frac{t^2}{\lambda}\zeta_h\right)\right\|_T^2,$$

$$\mu_4^2(T) := \sum_{\substack{F \in \mathcal{E} \\ F \subseteq T}} \frac{t^3}{\lambda^{3/2}\sqrt{E}} \min\left\{1, \frac{h_T\sqrt{\lambda}}{t\sqrt{E}}\right\} \|[\zeta_h]_F \cdot \tau_F\|_F^2,$$

$$\mu_5^2(T) := \left(\frac{h_T^2}{E^2} + \frac{t^2}{E\lambda}\right) \|\eta - \Pi_k \eta\|_T^2,$$

and the total local and global error estimator

$$\mu^2(T) := \sum_{j=1}^5 \mu_j^2(T) \qquad \text{and} \qquad \mu := \sqrt{\sum_{T \in \mathcal{T}} \mu^2(T)}.$$

The following main result states reliability and local efficiency of the error estimator up to data approximation errors.

**Theorem 2.** *The exact solution $(\phi, \alpha) \in [H_0^1(\Omega)]^2 \times H^1(\Omega)/\mathbb{R}$ and its discretization $(\phi_h, \alpha_h) \in \Phi_h \times Q_h$ satisfy*

$$|\phi - \phi_h|_1 + E^{-1}\|\alpha - \alpha_h\| + \frac{t}{\sqrt{E\lambda}}|\alpha - \alpha_h|_1 \lesssim \mu$$

*and*

$$\begin{aligned}\mu(T) \lesssim\ & |\phi - \phi_h|_{1,\omega_T} + E^{-1}\|\alpha - \alpha_h\|_{\omega_T} \\ & + \frac{t}{\sqrt{E\lambda}}|\alpha - \alpha_h|_{1,\omega_T} + \left(\frac{h_T}{E} + \frac{t}{\sqrt{E\lambda}}\right)\|\eta - \Pi_k\eta\|_{\omega_T},\end{aligned}$$

*where $\omega_T = \bigcup\{K \in \mathcal{T} \mid T \cap K \neq \emptyset\}$ is the element patch.*

*Proof.* The proof follows from a direct re-scaling of the result in Theorem 3 below in combination with (9). □

*Remark* 2. Theorem 2 measures the error $\phi - \phi_h$ in the $H^1$ seminorm. An error estimate in the energy norm corresponding to the form $a$ can be directly derived with Korn's inequality and the scaling $|\psi|_1 \approx E^{-1}\|\mathbb{C}^{1/2}\varepsilon(\psi)\|$ for any $\psi \in [H_0^1(\Omega)]^2$.

*Remark* 3. If $\eta \in H(\operatorname{div}, \Omega)$ is piecewise smooth and in a suitable finite-dimensional space allowing for discrete estimates, $\zeta_h$ can be replaced by $\tilde{\zeta}_h := \eta - \operatorname{Curl} \alpha_h$ in the definition of the error estimator. The differences in the error estimator can be estimated via an inverse and a trace inequality by $\mu_5$. Therefore, the two definitions are equivalent. However, for arbitrary $\eta \in H(\operatorname{div}, \Omega)$, the rotation and tangential jumps of $\eta$ do not exist in general.

*Remark* 4. The discretization of [GS20] employs a generalized Mini finite element pair for the discretization of $\Phi_h$ and $Q_h$ instead of the Taylor–Hood finite element pair in this paper. Since the discrete formulation then has the form (4), see also [GS20, Section 2.2.2], the proof of Theorem 2 carries over to this discretization as well.

### 2.4 Boundary conditions

The theory from the foregoing sections as well as that of [GS20, GS21] easily extends to other boundary conditions. Table 1 lists the most relevant boundary conditions following the exposition in [AF89b] and their implications on the nonstandard variables $\alpha$ and $\eta$ on the boundary. The boundary is assumed to be decomposed as

$$\partial\Omega = \Gamma_{\mathrm{hc}} \cup \Gamma_{\mathrm{sc}} \cup \Gamma_{\mathrm{hss}} \cup \Gamma_{\mathrm{sss}} \cup \Gamma_{\mathrm{f}}$$

in hard clamped (hc), soft clamped (sc), hard simply supported (hss), soft simply supported (sss), and free (f) parts, where we assume that $\Gamma_{\mathrm{f}}$ is connected. We assume that the edges of the triangulation match with this partition of the boundary and denote by $\mathcal{E}_{\mathrm{hc}}$, $\mathcal{E}_{\mathrm{sc}}$, $\mathcal{E}_{\mathrm{hss}}$, $\mathcal{E}_{\mathrm{sss}}$, $\mathcal{E}_{\mathrm{f}}$ the edges belonging to the respective parts of the boundary.

The modifications for the method and the a posteriori error estimator are described in this section. In absence of free boundary parts, only boundary conditions on $\phi$ are prescribed in the Schur complement while the boundary data of $\eta$ are not relevant and uniqueness of $\alpha$ is enforced by the usual condition $\int_\Omega \alpha = 0$. If the free boundary has positive surface measure, $\alpha$ satisfies homogeneous Dirichlet conditions there and $\eta$ must be chosen with vanishing normal trace on that part of the boundary. The proofs of [GS20, GS21] are easily adapted to these more complicated configurations. The same applies to the residual-based a posteriori error estimator. While the volume terms $\mu_1(T)$ and $\mu_3(T)$ are not modified, the terms $\mu_2(T)$ and $\mu_4(T)$ have different contributions for boundary edges. Let $R_F$ and $S_F$ denote the edge residuals from $\mu_2$ and $\mu_4$, respectively, see Section 3 for the precise definition. The term $\mu_2^2(T)$ then reads as

$$\sum_{\substack{F\in\mathcal{E}(\Omega)\cup\mathcal{E}(\Gamma_{\mathrm{f}})\\ \cup\mathcal{E}(\Gamma_{\mathrm{sss}})\\ F\subseteq T}} h_F\|R_F\|_F^2 + \sum_{\substack{F\in\mathcal{E}(\Gamma_{\mathrm{sc}})\\ F\subseteq T}} h_F\|R_F\cdot\tau_F\|_F^2 + \sum_{\substack{F\in\mathcal{E}(\Gamma_{\mathrm{hss}})\\ F\subseteq T}} h_F\|R_F\cdot\nu_F\|_F^2$$

while $\mu_4$ is written as

$$\mu_4^2(T) = (\kappa_T/d) \sum_{\substack{F\in\mathcal{E}\setminus\mathcal{E}(\Gamma_{\mathrm{f}})\\ F\subseteq T}} \|S_F\|_F^2$$

with $d = t\sqrt{E/\lambda}$ and $\kappa_T = \min\{1, h_T/d\}$ as in Section 3.

## 3 Proof of the main result

Since we are interested in error estimates uniform in the material parameters $E, t, \lambda$, we rewrite the system (2) in a dimensionless format with $\hat{a} = E^{-1}a$,

| | physical variables | | | our variables | | |
|---|---|---|---|---|---|---|
| | $\phi \cdot \tau$ | $\phi \cdot \nu$ | $w$ | $\alpha$ | $\eta \cdot \nu$ | natural BC |
| hc | 0 | 0 | 0 | — | — | — |
| sc | — | 0 | 0 | — | — | $\tau \cdot \boldsymbol{\sigma}\nu = 0$ |
| hss | 0 | — | 0 | — | — | $\nu \cdot \boldsymbol{\sigma}\nu = 0$ |
| sss | — | — | 0 | — | — | $\boldsymbol{\sigma}\nu = 0$ |
| free | — | — | — | 0 | 0 | $\boldsymbol{\sigma}\nu = 0$ and $(\nabla w - \phi) \cdot \nu = 0$ |

Table 1: Boundary conditions. We denote $\boldsymbol{\sigma} = \mathbb{C}\varepsilon(\phi)$.

$\hat{\mathbb{C}} = E^{-1}\mathbb{C}$, $\hat{\alpha} = E^{-1}\alpha$, $\hat{\alpha}_h = E^{-1}\alpha_h$, $f = E^{-1}\eta$, $g = -\lambda^{-1}t^2\eta$ and the rescaled thickness $d := t\sqrt{E/\lambda}$ as

$$\begin{aligned} \hat{a}(\phi, \psi) + b(\psi, \hat{\alpha}) &= (f, \psi)_{L^2(\Omega)} \\ b(\phi, \beta) - d^2\, c(\hat{\alpha}, \beta) &= b(g, \beta). \end{aligned} \tag{8}$$

By Korn's inequality [Bra07] the energy norm with respect to $\hat{a}$ is equivalent to the standard $H^1$ norm. The theory for saddle point problems with penalty term [Bra07] proves the equivalence of the error with the residual of the system (8), i.e.,

$$|\phi - \phi_h|_1 + \|\hat{\alpha} - \hat{\alpha}_h\|_{1,d} \approx \|\mathrm{Res}_1\|_{H^{-1}(\Omega)} + \|\mathrm{Res}_2\|_{(H^1(\Omega)/\mathbb{R})^\star,d} \tag{9}$$

with the residuals $\mathrm{Res}_1 \in ([H_0^1(\Omega)]^2)^\star$ and $\mathrm{Res}_2 \in (H^1(\Omega)/\mathbb{R})^\star$ defined by

$$\begin{aligned} \mathrm{Res}_1(\psi) &:= \hat{a}(\phi_h, \psi) + b(\psi, \hat{\alpha}_h) - (f, \psi)_{L^2(\Omega)}, \\ \mathrm{Res}_2(\beta) &:= b(\phi_h, \beta) - d^2 c(\hat{\alpha}_h, \beta) - b(g, \beta) \end{aligned}$$

for all $\psi \in [H_0^1(\Omega)]^2$ and $\beta \in H^1(\Omega)/\mathbb{R}$. Here,

$$\|\beta\|_{1,d} := \|\beta\| + d\,|\beta|_1 \quad \text{and} \quad \|F\|_{(H^1(\Omega)/\mathbb{R})^\star,d} := \sup_{v \in (H^1(\Omega)/\mathbb{R})\setminus\{0\}} \frac{F(v)}{\|v\|_{1,d}}.$$

For a triangle $T \in \mathcal{T}$ and an edge $F \in \mathcal{E}$ we define the local residuals as

$$\begin{aligned} R_T &:= (-\operatorname{div} \hat{\mathbb{C}}\varepsilon(\phi_h) + \operatorname{Curl} \hat{\alpha}_h - \Pi_k f)|_T, & R_F &:= [\hat{\mathbb{C}}\varepsilon(\phi_h)]_F \nu_F, \\ S_T &:= \operatorname{rot}(\phi_h - d^2 \operatorname{Curl} \hat{\alpha}_h - \Pi_k g)|_T, & S_F &:= [\phi_h - d^2 \operatorname{Curl} \hat{\alpha}_h - \Pi_k g]_F \cdot \tau_F. \end{aligned}$$

We define

$$\kappa_T = \min\{1, h_T/d\}.$$

Define the local error estimator contributions

$$\begin{aligned} \hat{\mu}_1(T) &:= h_T \|R_T\|_T + h_T \|(f - \Pi_k f)\|_T, & \hat{\mu}_3(T) &:= \kappa_T \|S_T\|_T + d^{-1} \|g - \Pi_k g\|_T, \\ \hat{\mu}_2(T) &:= \sqrt{\sum_{\substack{F \in \mathcal{E}(\Omega) \\ F \subseteq T}} h_F \|R_F\|_F^2}, & \hat{\mu}_4(T) &:= (\kappa_T/d)^{1/2} \sqrt{\sum_{\substack{F \in \mathcal{E} \\ F \subseteq T}} \|S_F\|_F^2}. \end{aligned}$$

The following result proves the reliability and efficiency of the error estimator for the rescaled system.

**Theorem 3.** *The error estimator is reliable and efficient in the sense that*

$$\begin{aligned}\|\mathrm{Res}_1\|_{H^{-1}(\Omega)} &\lesssim \sqrt{\sum_{T\in\mathcal{T}} \big(\hat\mu_1^2(T)+\hat\mu_2^2(T)\big)},\\ \|\mathrm{Res}_2\|_{(H^1(\Omega)/\mathbb{R})^\star,d} &\lesssim \sqrt{\sum_{T\in\mathcal{T}} \big(\hat\mu_3^2(T)+\hat\mu_4^2(T)\big)}\end{aligned} \tag{10}$$

*and, for any $T\in\mathcal{T}$,*

$$\begin{aligned}\hat\mu_1(T)+\hat\mu_2(T) &\lesssim |\phi-\phi_h|_{1,\omega_T}+\|\hat\alpha-\hat\alpha_h\|_{\omega_T}+\|h_T(f-\Pi_k f)\|_{\omega_T},\\ \hat\mu_3(T)+\hat\mu_4(T) &\lesssim \kappa_T|\phi-\phi_h|_{1,\omega_T}+d\,|\hat\alpha-\hat\alpha_h|_{1,\omega_T}+d^{-1}\|g-\Pi_k g\|_{\omega_T}.\end{aligned}$$

*Proof.* ***Proof of reliability, first part.*** Let $\psi\in[H^1_0(\Omega)]^2$ with $\|\nabla\psi\|=1$ be arbitrary. Let $\psi_h\in\Phi_h$ be an $L^2$-stable quasi-interpolation [Ver13] of $\psi$. The discrete equation (4) shows that $\mathrm{Res}_1(\psi_h)$ equals $-(f-\Pi_k f,\psi_h)_{L^2(\Omega)}$. Therefore, a piecewise integration by parts and the continuity of $e_\psi:=\psi-\psi_h$ prove

$$\begin{aligned}\mathrm{Res}_1(\psi)&=\mathrm{Res}_1(e_\psi)-(f-\Pi_k f,\psi_h)_{L^2(\Omega)}\\ &=\sum_{T\in\mathcal{T}}(R_T,e_\psi)_{L^2(T)}+\sum_{F\in\mathcal{E}(\Omega)}(R_F,e_\psi)_{L^2(F)}-(f-\Pi_k f,\psi)_{L^2(T)}.\end{aligned}$$

A weighted Cauchy inequality reveals

$$\begin{aligned}\mathrm{Res}_1(\psi)\le\sum_{T\in\mathcal{T}}\|h_T R_T\|_T\,\|h_T^{-1}e_\psi\|_T+\sum_{F\in\mathcal{E}(\Omega)}\|R_F\|_F\,\|e_\psi\|_F\\ +\sum_{T\in\mathcal{T}}\|h_T(f-\Pi_k f)\|_T\|h_T^{-1}(\psi-\Pi_k\psi)\|_T.\end{aligned}$$

The trace inequality [Ver13, Remark 3.6], the approximation properties of $\psi_h$, and standard estimates imply the claimed bound.

***Proof of reliability, second part.*** Let now $\beta\in H^1(\Omega)/\mathbb{R}$ be given with $\|\beta\|_{1,d}=1$ and $\beta_h\in Q_h$ its quasi-interpolant. We write $e_\beta:=\beta-\beta_h$. The inclusion $Q_h\subseteq\ker(\mathrm{Res}_2)$ from (4) proves

$$\mathrm{Res}_2(\beta)=\mathrm{Res}_2(e_\beta)=(\phi_h-d^2\,\mathrm{Curl}\,\hat\alpha_h-\Pi_k g,\mathrm{Curl}\,e_\beta)_{L^2(\Omega)}+b(g-\Pi_k g,e_\beta).$$

Integration by parts yields

$$\mathrm{Res}_2(\beta)=-\sum_{T\in\mathcal{T}}(S_T,e_\beta)_{L^2(T)}+\sum_{F\in\mathcal{E}}(S_F,e_\beta)_{L^2(F)}+b(g-\Pi_k g,e_\beta). \tag{11}$$

The approximation properties of the quasi interpolant [Ver13]

$$\|e_\beta\|_T\lesssim\min\{\|\beta\|_{\omega_T},h_T|\beta|_{1,\omega_T}\}\quad\text{and}\quad|e_\beta|_{1,T}\lesssim|\beta|_{1,\omega_T} \tag{12a}$$

prove

$$h_T^{-1/2}\|e_\beta\|_T\lesssim\sqrt{\|\beta\|_{\omega_T}\,|\beta|_{1,\omega_T}}\quad\text{and}\quad\|e_\beta\|_T\lesssim\kappa_T\|\beta\|_{1,d,T} \tag{12b}$$

for the local norm

$$\|\beta\|_{1,d,T} := \|\beta\|_T + d|\beta|_{1,T}.$$

The multiplicative trace inequality and the Young inequality therefore prove

$$\|e_\beta\|_F \lesssim h_F^{-1/2}\|e_\beta\|_{T_F} + \|e_\beta\|_{T_F}^{1/2}\,|e_\beta|_{1,T_F}^{1/2} \lesssim d^{-1/2}\|\beta\|_{\omega_{T_F}} + d^{1/2}|\beta|_{1,\omega_{T_F}}$$

for any $T_F \in \mathcal{T}$ with $F \subseteq T$. On the other hand, the standard trace inequality and (12) lead to

$$\|e_\beta\|_F \lesssim h_F^{-1/2}\|e_\beta\|_{T_F} + h_F^{1/2}|e_\beta|_{1,T_F} \lesssim h_F^{1/2}|\beta|_{1,\omega_{T_F}}.$$

Hence,

$$\|e_\beta\|_F \lesssim \min\{d^{-1/2}, h_F^{1/2}/d\}\ \|\beta\|_{1,d,\omega_{T_F}} \approx (\kappa_{T_F}/d)^{1/2}\ \|\beta\|_{1,d,\omega_{T_F}}.$$

Therefore, the second term in (11) can be estimated as

$$\sum_{F\in\mathcal{E}} (S_F, e_\beta)_{L^2(F)} \lesssim \sqrt{\sum_{T\in\mathcal{T}} \sum_{\substack{F\in\mathcal{E}\\ F\subseteq\partial T}} d^{-1}\kappa_T\,\|S_F\|_F^2}.$$

This and (12b) and standard estimates for the remaining terms of (11) show the second estimate of (10).

***Proof of efficiency of*** $\hat\mu_1$ ***and*** $\hat\mu_2$**.** Since the volume residual can be rewritten as

$$R_T = \big(-\operatorname{div}(\mathbb{C}\varepsilon(\phi_h) - \hat\alpha_h I^\perp) - \Pi_k f\big)|_T \quad \text{with } I^\perp = \left[\begin{smallmatrix} 0 & -1 \\ 1 & 0 \end{smallmatrix}\right],$$

well-known local efficiency estimates [Ver13] show the stated bound for $\hat\mu_1$, $\hat\mu_2$.

***Proof of efficiency of*** $\hat\mu_3$**.** To this end, define the volume bubble $\flat_T \in H_0^1(T)$ by $\flat_T := \lambda_1\lambda_2\lambda_3$ for the barycentric coordinates $\lambda_j$, $j = 1,2,3$ of $T$ and let $\varphi := \flat_T S_T$. Equivalence of norms and the second equation of (8) with piecewise integration by parts lead to

$$\|S_T\|_{L^2(T)}^2 \approx (S_T,\varphi)_{L^2(T)} = b(\phi-\phi_h,\varphi) - d^2\,c(\hat\alpha-\hat\alpha_h,\varphi) - b(g-\Pi_k g,\varphi).$$

The local support and the scaling of $\varphi$ then lead to

$$\kappa_T\,\|S_T\|_T \lesssim \kappa_T\,|\phi-\phi_h|_{1,T} + d|\hat\alpha-\hat\alpha_h|_{1,T} + d^{-1}\|g-\Pi_k g\|_T \tag{13}$$

where we used the elementary formula $d\kappa_T/h_T \le 1$.

***Proof of efficiency of*** $\hat\mu_4$**.** Similar to [Ver98, Ver13], we define the $d$-dependent edge bubble $\flat_{F,d}$ in the following way. For any $T = \operatorname{conv}\{a,b,c\} \in \mathcal{T}$ and any edge $F = \operatorname{conv}\{a,b\} \in \mathcal{E}(T)$, define the triangle $K_{T,d}$ by

$$K_{T,d} = T \quad \text{if } d \ge h_{T,F}, \qquad \text{and} \qquad K_{T,d} = \operatorname{conv}\{a,b,c_d\} \quad \text{if } d < h_{T,F},$$

where $c_d = (a+b)/2 + d(c-(a+b)/2)$ and $h_{T,F} = |c-(a+b)/2|$, see Figure 1. In what follws, we fix $T \in \mathcal{T}$ and an edge $F$ of $T$ and will bound $\hat\mu_4(T)$. If $F$ is an interior edge, let $T_+, T_- \in \mathcal{T}$ denote the two triangles with $F = T_+ \cap T_-$ (one of them being $T$). Let $\flat_{F,d} \in H_0^1(\Omega)$ be the edge bubble of $F$ with respect

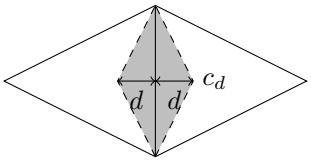


Figure 1: Subtriangles for $d < h_T$.

to the triangles $K_{T_+,d}$ and $K_{T_-,d}$. In particular, $\operatorname{supp}(\flat_{F,d}) = \overline{\omega}_{F,d}$ with $\omega_{F,d} := \operatorname{int}(K_{T_+,d} \cup K_{T_-,d})$. Moreover, $\|\flat_{F,d}\|_{L^\infty(\Omega)} \leq 1$ and

$$\|\nabla \flat_{F,d}\|_{L^\infty(\Omega)} \lesssim \min\{d, h_T\}^{-1} \approx (d\kappa_T)^{-1}. \tag{14}$$

Let $J \in H^1(\omega_{F,d})$ be a continuation of $S_F$ that is constant in the normal direction. Define $\varphi := \flat_{F,d} J \in H^1_0(\omega_{F,d})$. Then

$$\|\varphi\| \leq \|J\|_{\omega_{F,d}} \lesssim \min\{d, h_T\}^{1/2} \|J\|_F \approx (d\kappa_T)^{1/2} \|J\|_F. \tag{15}$$

Moreover, the product rule, the properties of the continuation $J$, an inverse inequality along $F$, and the scaling property (14) imply

$$\begin{aligned} \|\nabla\varphi\| &\lesssim \|\nabla J\|_{\omega_{F,d}} + (d\kappa_T)^{-1} \|J\|_{\omega_{F,d}} \\ &\lesssim \min\{d, h_T\}^{1/2} (\|\partial J/\partial\tau\|_F + (d\kappa_T)^{-1} \|J\|_F) \\ &\lesssim (d\kappa_T)^{-1/2} \|J\|_F, \end{aligned} \tag{16}$$

where for the last step, elementary calculations show $h_T^{-1} (d\kappa_T)^{1/2} \leq (d\kappa_T)^{-1/2}$. We abbreviate $Z := \phi_h - d^2 \operatorname{Curl} \hat\alpha_h - \Pi_k g$. Equivalence of norms and integration by parts lead to

$$\|S_F\|_F^2 = ([Z]_F \cdot \tau_F, \varphi)_{L^2(F)} = (Z, \operatorname{Curl}\varphi)_{L^2(\omega_{F,d})} + (\operatorname{rot}_{\mathcal{T}} Z, \varphi)_{L^2(\omega_{F,d})}. \tag{17}$$

Let $\omega_F = T_+ \cup T_-$ denote the patch of $F$. The second equation of (8) proves for the first term on the right-hand side that

$$\begin{aligned} &(Z, \operatorname{Curl}\varphi)_{L^2(\omega_{F,d})} \\ &\quad = -b(\phi - \phi_h, \varphi) + d^2\, c(\hat\alpha - \hat\alpha_h, \varphi) + b(g - \Pi_k g, \varphi) \\ &\quad \leq |\phi - \phi_h|_{1,\omega_F} \|\varphi\| + d^2 |\hat\alpha - \hat\alpha_h|_{1,\omega_F} \|\nabla\varphi\| + \|g - \Pi_k g\|_{\omega_F} \|\nabla\varphi\| \\ &\quad \lesssim \|J\|_F \Big( (d\kappa_T)^{1/2} |\phi - \phi_h|_{1,\omega_F} + (d\kappa_T)^{-\frac12} (d^2 |\hat\alpha - \hat\alpha_h|_{1,\omega_F} + \|g - \Pi_k g\|_{\omega_F}) \Big), \end{aligned}$$

where we used the scaling (15)–(16) of $\varphi$ in the last step. The Cauchy inequality and the scaling (15) lead for the second term on the right-hand side of (17) to

$$(\operatorname{rot}_{\mathcal{T}} Z, \varphi)_{L^2(\omega_{F,d})} = \sum_{K=T_+,T_-} (S_K, \varphi)_{L^2(K)} \lesssim (d\kappa_T)^{1/2} \|J\|_F \sum_{K=T_+,T_-} \|S_K\|_K.$$

The combination of the foregoing three displayed formulae with the bound (13) reveals

$$(\kappa_T/d)^{1/2} \|S_F\|_F \lesssim \kappa_T |\phi - \phi_h|_{1,\omega_F} + d |\hat\alpha - \hat\alpha_h|_{1,\omega_F} + d^{-1} \|g - \Pi_k g\|_{\omega_F}.$$

If $F$ is a boundary edge, the proof follows the same lines with $T_- = \emptyset$. Summation over the edges of $T$ then proves the stated efficiency of $\hat\mu_4(T)$. □

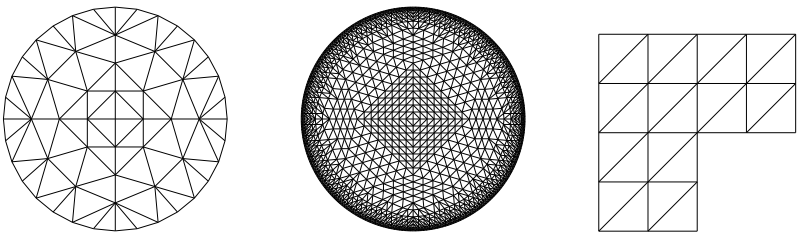

Figure 2: Initial triangulation and mesh after two refinements of the experiment from Section 4.1 and initial triangulation of the experiment from Section 4.2.

*Remark* 5. Estimate (13) reveals the sharper efficiency bound

$$\hat{\mu}_3(T) \lesssim \kappa_T \, |\phi - \phi_h|_{1,T} + \min\{1, d/h_T\} d |\hat{\alpha} - \hat{\alpha}_h|_{1,T} + \min\{h_T^{-1}, d^{-1}\} \|g - \Pi_k g\|_T.$$

# 4 Numerical results

This section is devoted to two numerical experiments. In the experiments, the error estimator was computed with $\eta$ instead of $\Pi_k \eta$. According to Remark 3, these two quantities are equivalent. We refrain from introducing new symbols for these slightly modified estimators and simply use the notation $\mu_1, \dots, \mu_5$ for the global estimators $\mu_j := \sqrt{\sum_{T \in \mathcal{T}} \mu_j^2(T)}$. Let $h := \max\{h_T \mid T \in \mathcal{T}\}$ denote the maximal mesh-size of $\mathcal{T}$.

## 4.1 Disc domain with exact solution

We consider the solution provided by [AF89b] for the unit disc $\Omega = \{x^2 + y^2 < 1\}$ with simply supported boundary $\Gamma_{\text{sss}} = \partial\Omega$. In this example, the exact solution is known and the exact error can be compared to the error estimator. The precise data can be found in Appendix A. We choose the material parameters as $E = 1000$, $\nu = 0.3$, $\kappa = 5/6$.

As explained in [AF89b, AF90], in this case $D^{2+k}\phi$ is of order $t^{-(k+1)}$ in a strip of width proportional to $t$ close to the boundary for $k = 0, 1$. This implies $\|D^{2+k}\phi\| \approx t^{-(k+1/2)}$. The error bound involving $h^{k+1}\|D^{2+k}\phi\|$ therefore suggests that asymptotic convergence can be observed is visible for $h \lesssim t^{1/2}$ if $k = 0$ and for $h \lesssim t^{3/4}$ if $k = 1$.

To resolve the curved boundary of $\Omega$, we choose polygonal approximations from the interior and the following mesh refinement method: uniform mesh refinement (red refinement), after which the resulting boundary vertices are projected to the boundary $\partial\Omega$, is followed by one local refinement of all elements near the boundary. More precisely, we mark all triangles containing a boundary vertex and refine with newest-vertex bisection [Ver13], and then project new boundary points to the boundary of $\Omega$. Since in all diagrams, the symbol $h$ refers to the maximal mesh size, the locally refined meshes have a resolution of order $h^2$ near the boundary. The initial triangulation and the triangulation with maximal mesh-size $h = \sqrt{2}/16$ is displayed in Figure 2.

The convergence history of the errors and error estimators for the discretization for $k = 0$ and $k = 1$ is plotted in Figure 3 for $t = 1$ and in Figure 4

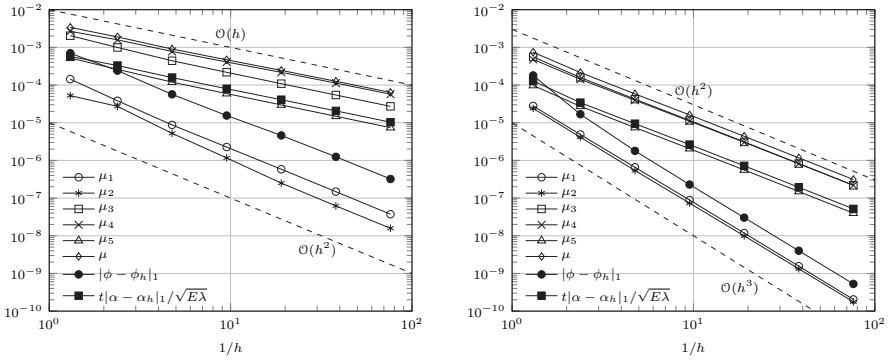


Figure 3: Numerical results for the disc domain $t = 1$ for $k = 0$ (left) and $k = 1$ (right) from Subsection 4.1.

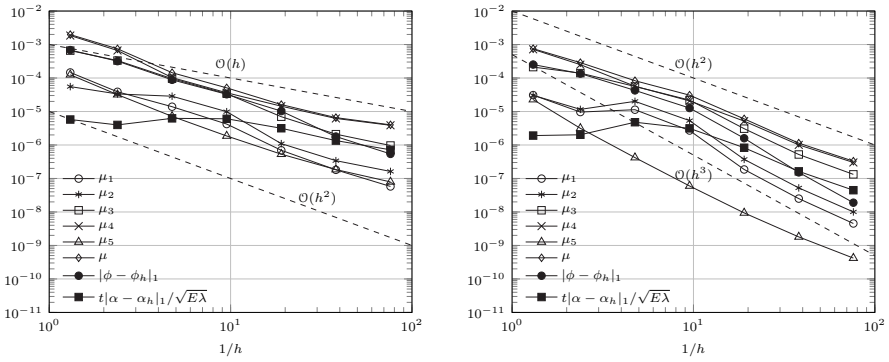


Figure 4: Numerical results for the disc domain $t = 1/100$ for $k = 0$ (left) and $k = 1$ (right) from Subsection 4.1.

for $t = 1/100$. The error $|\phi - \phi_h|_1$ shows a convergence rate of $h^{k+2}$ in all experiments as predicted by [GS21], while the error $t|\alpha - \alpha_h|/\sqrt{E\lambda}$ converges with rate $h^{k+1}$. Moreover, $t|\alpha - \alpha_h|/\sqrt{E\lambda}$ shows for $t = 1/100$ a preasymptotic stagnation and the start of the asymptotic convergence rate can be observed for approximately $h = 1/10$. The single parts of the error estimator also converge with different convergence rates. While $\mu_1$ and $\mu_2$ converge with rate $h^{k+2}$ for $t = 1$, the error estimator parts $\mu_3$, $\mu_4$, and $\mu_5$ converge with rate $h^{k+1}$. While in the efficiency bound of $\mu_3$ and $\mu_4$ in Theorem 3 the norm $t|\alpha - \alpha_h|_1/\sqrt{E\lambda}$ enters, the upper bound for $\mu_1$ and $\mu_2$ contains only the $L^2$ norm of the error in $\alpha$. The right-hand side in this example possesses the smoothness $\eta \in H^{2-\varepsilon}(\Omega)$ for any $\varepsilon > 0$, which explains the convergence order $h^{k+1}$ with $k = 0, 1$ for $\mu_5$. For $t = 1/100$, the observed asymptotic convergence rates are similar for $k = 2$, but the convergence starts after a preasymptotic range. For $k = 0$, the range of mesh sizes under consideration seems not sufficient for observing the asymptotic convergence order $h$ in the case $t = 1/100$.

## 4.2 L-shaped domain

We consider the domain $\Omega = (-1, 1)^2 \setminus ([0, 1] \times [-1, 0])$ with hard clamped boundary $\Gamma_{\mathrm{hc}} = \{0\} \times [-1, 0] \cup [0, 1] \times 0$ and free boundary $\Gamma_{\mathrm{f}} = \partial\Omega \setminus \Gamma_{\mathrm{hc}}$. The vertical force $\ell$ takes the value $-16$ on the square $(-\frac{3}{4}, -\frac{1}{2})^2$ and 0 elsewhere. Accordingly, $\eta$ is chosen as

$$\eta(x) = \begin{cases} (\min\{4, 16x_1 + 12\}, 0) & \text{if } x_1 > -\frac{3}{4} \text{ and } -\frac{3}{4} < x_2 < -\frac{1}{2}, \\ 0 & \text{otherwise.} \end{cases}$$

The material parameters are chosen as $E = 1000$, $\nu = 0.3$ and $\kappa = 5/6$.

The discrete solutions and their error estimator terms are computed on a sequence of uniformly refined meshes and on a sequence of meshes refined by an adaptive algorithm with the steps *Solve*, *Estimate*, *Mark*, *Refine*. The error estimator $\mu$ is used in the Dörfler marking with bulk parameter $1/2$, see [Ver13] for details. The initial triangulation is displayed in Figure 2. In the numerical example from Subsection 4.1, the quality of the approximation was bounded by the approximation of the circle and therefore, we restricted the presented experiments to $k = 0$ and $k = 1$. In contrast to that, the full approximation properties for $k = 2$ can be utilized in this example, and therefore the shown results are mostly for $k = 0$ and $k = 2$.

The adaptively generated meshes for $k = 0$ and $k = 2$ and for $t = 1$ and $t = 1/100$ with approximately 7000 elements can be found in Figure 5. The mesh-refinement for $t = 1$ occurs mostly at three places: Near the square $(-\frac{3}{4}, -\frac{1}{2})^2$, where the force does not vanish, at the re-entrant corner $(0, 0)$, and at some of the other corners. The mesh-refinement at the re-entrant corner seems to be stronger than at the other corners, which is in accordance with the local regularity predicted by [RS11] which is $H^{1+s}(\omega_z)$ for some neighborhood $\omega_z$ of $(0, 0)$ for $s = 0.60404435890$. In comparison to that, the predicted local regularity at the corners $(0, -1)$ and $(1, 0)$ is $s = 0.75834915$, while for the other corners it is $s = 1$. Possibly due to the force that concentrates on the lower left of the domain, the corner $(1, 0)$ is not refined for $k = 0$, while a slight mesh-refinement can be observed at $(0, -1)$. Since local $H^2$ regularity is not enough to exploit the full approximation properties for $k = 2$, we expect a local refinement

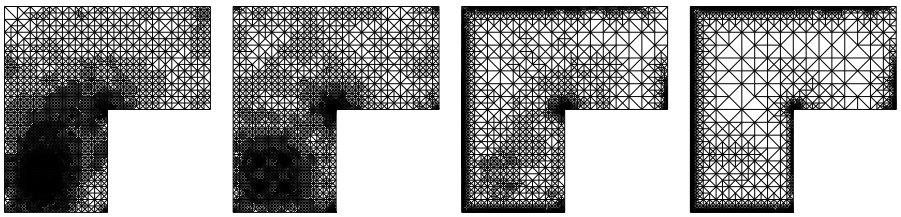

(a) (b) (c) (d)

Figure 5: Adaptively generated triangulations with approximately 7000 elements for $k = 0$ and $t = 1$ (a), $k = 2$ and $t = 1$ (b), $k = 0$ and $t = 1/100$ (c), and $k = 2$ and $t = 1/100$ (d).

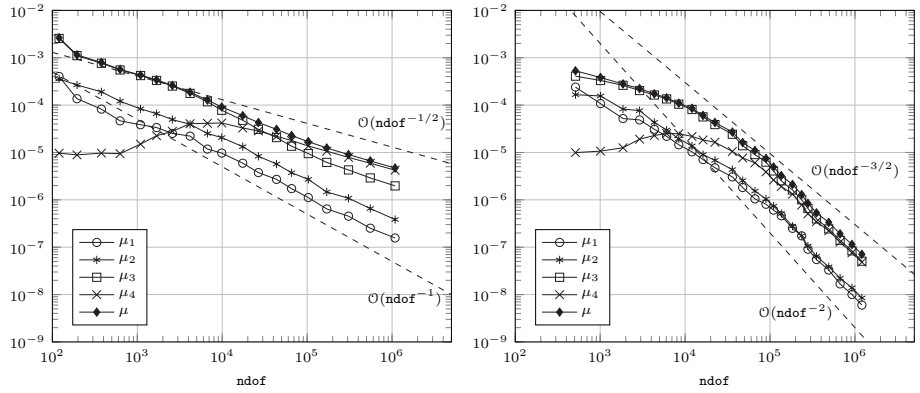


Figure 6: The different error estimator terms for $t = 1/100$ and $k = 0$ (left) and $k = 1$ (right) on adaptively refined meshes for the numerical experiment on the L domain from Subsection 4.2. When $(-\frac{3}{4}, -\frac{1}{2})$ is resolved by the triangulation, the oscillations of $\eta$ vanish and are therefore not included in the diagram.

at all corners for $k = 2$, which can in fact be observed. Moreover, for $k = 2$ the refinement in the interior is not more or less equally distributed at the whole square $(-\frac{3}{4}, -\frac{1}{2})^2$ as for $k = 0$, but it is concentrated at the corners of that square. For $t = 1/100$ the solution develops a boundary layer and therefore, the mesh-refinement concentrates at the boundary layer and at the singularity at the re-entrant corner, but hardly any mesh-refinement takes place in the interior of the domain, especially for $k = 2$. While for $k = 0$, the mesh-refinement at the boundary is only observed at the free boundary, the mesh-refinement for $k = 2$ takes place also at parts of the hard clamped boundary. This conforms to the theory of [AF90] where it is explained that the boundary layer at the hard clamped boundary does not affect the first two derivatives of $\phi$. This is why the low-order approximation with $k = 0$ does not suffer from a boundary layer effect in the hard-clamped configuration, in contrast to the case $k = 2$, where higher-order derivatives of $\phi$ enter the approximation bounds and scale with negative powers of the thickness $t$.

In Figure 6, the single error estimator terms for $t = 1/100$ and $k = 0$ and

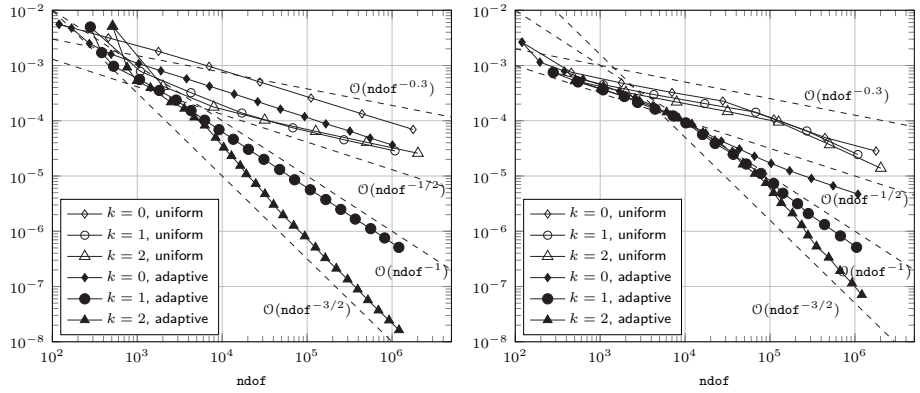


Figure 7: The error estimator on uniform and adaptively refined meshes for $k = 0, 1, 2$ and $t = 1$ (left) and $t = 1/100$ (right) for the numerical experiment on the L domain from Subsection 4.2.

$k = 2$ on adaptively refined meshes are plotted against the number of degrees of freedom. The error estimator term $\mu_4$ shows after a large preasymptotic stagnation up to approximately $10^5$ degrees of freedom a convergence rate of $\mathtt{ndof}^{-(k+1)/2}$. The error estimator term $\mu_3$ shows for $k = 2$ also a convergence rate of $\mathtt{ndof}^{-(k+1)/2}$, while for $k = 0$ it is slightly larger, which is in accordance with Remark 5. The error estimator terms $\mu_1$ and $\mu_2$ show as in the numerical example of Subsection 4.1 a better convergence rate of almost $\mathtt{ndof}^{-(k+2)/2}$. The superconvergence result of [GS21] applies in general also to non-uniform meshes. However, the superconvergence is only with respect to the maximal mesh-size to the power $s$, where $s$ is the elliptic regularity constant for the Poisson–Neumann problem, in this case the limiting regularity is $s = 2/3$. The superior convergence rate of $\mu_1$ and $\mu_2$ could be a hint towards the superconvergence of the error in $\phi$. Since only the whole error estimator is an upper bound of the error in $\phi$, it is, however, an open question, whether the error in $\phi$ shows a better superconvergence behaviour as predicted by the theory.

In Figure 7 the error estimator $\mu$ is plotted against the number of degrees of freedom for $k = 0, 1, 2$ and $t = 1$ and $t = 1/100$ on uniformly and adaptively refined meshes. For $t = 1$, the error estimator for $k = 1$ and $k = 2$ show a convergence rate of $\mathtt{ndof}^{-0.3}$ on uniform meshes, while for $k = 0$, a better convergence rate of $\mathtt{ndof}^{-0.5}$ is observed. However, as $\mu$ lies still above the error estimator for $k = 1$ and $k = 2$ on uniform meshes, it is assumed that the better convergence rate is only a preasymptotic effect. The convergence rate is in accordance to the predicted regularity of $H^{1+s}(\Omega)$ with $s = 0.6\ldots$ as above. For $k = 0$, it seems that the adaptive refinement has no effect on the convergence rate in this still preasymptotic regime. For $k = 1$ and $k = 2$, a clear improvement to the optimal convergence rate $\mathtt{ndof}^{-(k+1)/2}$ can be observed for adaptively refined meshes. For $t = 1/100$ the same asymptotic convergence rates are observed except for the uniform refinement for $k = 1$ and $k = 2$. In these two cases, the error estimator shows a convergence rate between $1/2$ and 1 in terms of number of degrees of freedom. This is probably due to the unresolved boundary layer for the uniform mesh-refinement. In contrast to $t = 1$, all error estimator terms show a preasymptotic worse convergence rate

up to approximately $10^5$ degrees of freedom.

# A Collection of formulas

The exact solution from [AF89b, Table 4] is given in polar coordinates $(r, \theta)$ as follows. Given the material parameters $E$, $\nu$, $\kappa$, and the thickness parameter $t$, define the constants

$$\lambda = (1+\nu)^{-1} E\kappa/2, \quad \mathbb{D} = E/(12(1-\nu^2)), \quad \boldsymbol{\alpha} = \sqrt{12\kappa}.$$

Given the right-hand side $\ell(r,\theta) = \cos\theta$, the rotation $\phi$ (given in radial and angular parts) and the displacement $w$ read

$$\begin{aligned}
\phi_r &= [4r^3/(45\mathbb{D}) + 3\boldsymbol{a}r^2 + \boldsymbol{b} - \boldsymbol{c}\lambda^{-1}t^2 + r^{-1}\lambda^{-1}\boldsymbol{d}t^2 I_1(\boldsymbol{\alpha}r/t)]\cos\theta \\
\phi_\theta &= [-r^3/(45\mathbb{D}) - \boldsymbol{a}r^2 - \boldsymbol{b} + \boldsymbol{c}\lambda^{-1}t - \boldsymbol{d}\boldsymbol{\alpha}\lambda^{-1}tI_1'(\boldsymbol{\alpha}r/t)]\sin\theta \\
w &= [r^4/(45\mathbb{D}) - \lambda^{-1}t^2r^2/3 + \boldsymbol{a}(r^3 - 8\mathbb{D}\lambda^{-1}rt^2) + \boldsymbol{b}r - \boldsymbol{c}\lambda^{-1}t^2 r]\cos\theta.
\end{aligned}$$

Here, $I_1$ is the modified Bessel function of the first kind [AS64] of order 1, and the functions involved in these expressions are given as follows

$$\begin{aligned}
\boldsymbol{f} &= 15[(3\boldsymbol{\alpha}^2 + \boldsymbol{\alpha}^2\nu + 8t^2)I_1(\boldsymbol{\alpha}/t) - 8\boldsymbol{\alpha}tI_1'(\boldsymbol{\alpha}/t)], \\
\boldsymbol{a} &= [-(4\boldsymbol{\alpha}^2 + \boldsymbol{\alpha}^2\nu + 10t^2)I_1(\boldsymbol{\alpha}/t) + 10\boldsymbol{\alpha}tI'(\boldsymbol{\alpha}/t)]/(2\mathbb{D}\boldsymbol{f}), \\
\boldsymbol{b} &= [(6\boldsymbol{\alpha}^2 + \boldsymbol{\alpha}^2\nu + 14t^2)I_1(\boldsymbol{\alpha}/t) - 14\boldsymbol{\alpha}tI_1'(\boldsymbol{\alpha}/t)]/(6\mathbb{D}\boldsymbol{f}), \\
\boldsymbol{c} &= \boldsymbol{\alpha}^2(1-\nu)I_1(\boldsymbol{\alpha}/t)/\boldsymbol{f}, \qquad \boldsymbol{d} = 2\lambda/(\mathbb{D}\boldsymbol{f}).
\end{aligned}$$

Note that $\eta(r,\theta) = r\begin{pmatrix} \sin^2(\theta) \\ -\sin(\theta)\cos(\theta) \end{pmatrix}$ satisfies $-\operatorname{div}\eta = \ell$.

# References


[AF89a] D. N. Arnold and R. S. Falk. A uniformly accurate finite element method for the Reissner-Mindlin plate. *SIAM J. Numer. Anal.*, 26(6):1276–1290, 1989.

[AF89b] Douglas N. Arnold and Richard S. Falk. Edge effects in the Reissner-Mindlin plate theory. In A. K. Noor, T. Belytschhko, and J.C. Simo, editors, *Analytic and Computational Models of Shells*, pages 71–90. A.S.M.E., New York, 1989.

[AF90] D. N. Arnold and R. S. Falk. The boundary layer for the Reissner-Mindlin plate model. *SIAM J. Math. Anal.*, 21(2):281–312, 1990.

[AS64] Milton Abramowitz and Irene A. Stegun. *Handbook of mathematical functions with formulas, graphs, and mathematical tables*, volume 55 of *National Bureau of Standards Applied Mathematics Series*. Washington, D.C., 1964.

[BBF13] D. Boffi, F. Brezzi, and M. Fortin. *Mixed finite element methods and applications*, volume 44 of *Springer Series in Computational Mathematics*. Springer, Heidelberg, 2013.

[BF86] F. Brezzi and M. Fortin. Numerical approximation of Mindlin-Reissner plates. *Math. Comp.*, 47(175):151–158, 1986.

[Bra07] D. Braess. *Finite Elements. Theory, Fast Solvers, and Applications in Elasticity Theory*. Cambridge University Press, Cambridge, third edition, 2007.

[Car02] C. Carstensen. Residual-based a posteriori error estimate for a nonconforming Reissner-Mindlin plate finite element. *SIAM J. Numer. Anal.*, 39(6):2034–2044, 2002.

[CH08] C. Carstensen and J. Hu. A posteriori error analysis for conforming MITC elements for Reissner-Mindlin plates. *Math. Comp.*, 77(262):611–632, 2008.

[CR73] M. Crouzeix and P.-A. Raviart. Conforming and nonconforming finite element methods for solving the stationary Stokes equations. I. *Rev. Française Automat. Informat. Recherche Opérationnelle Sér. Rouge*, 7(R-3):33–75, 1973.

[CS06] C. Carstensen and J. Schöberl. Residual-based a posteriori error estimate for a mixed Reißner-Mindlin plate finite element method. *Numer. Math.*, 103(2):225–250, 2006.

[CW01] C. Carstensen and K. Weinberg. Adaptive mixed finite element method for Reissner-Mindlin plate. *Comput. Methods Appl. Mech. Engrg.*, 190(51-52):6895–6908, 2001.

[CW03] C. Carstensen and K. Weinberg. An adaptive non-conforming finite-element method for Reissner-Mindlin plates. *Internat. J. Numer. Methods Engrg.*, 56(15):2313–2330, 2003.

[GS20] D. Gallistl and M. Schedensack. A robust discretization of the Reissner–Mindlin plate with arbitrary polynomial degree. *J. Comput. Math.*, 38:1–13, 2020.

[GS21] Dietmar Gallistl and Mira Schedensack. Taylor-Hood discretization of the Reissner-Mindlin plate. *SIAM J. Numer. Anal.*, 59(3):1195–1217, 2021.

[HH10] Jun Hu and Yunqing Huang. A posteriori error analysis of finite element methods for Reissner-Mindlin plates. *SIAM J. Numer. Anal.*, 47(6):4446–4472, 2010.

[RS11] Andreas Rössle and Anna-Margarete Sändig. Corner singularities and regularity results for the Reissner/Mindlin plate model. *J. Elasticity*, 103(2):113–135, 2011.

[Sch17] M. Schedensack. A new generalization of the $P_1$ non-conforming FEM to higher polynomial degrees. *Comput. Methods Appl. Math.*, 17(1):161–185, 2017.

[Ver98] R. Verfürth. Robust a posteriori error estimators for a singularly perturbed reaction-diffusion equation. *Numer. Math.*, 78(3):479–493, 1998.

[Ver13] Rüdiger Verfürth. *A posteriori error estimation techniques for finite element methods*. Numerical Mathematics and Scientific Computation. Oxford University Press, Oxford, 2013.